Contents lists available at ScienceDirect

Materials Characterization

journal homepage: www.elsevier.com/locate/matchar

Edge interfaces of the Ω plates in a peak-aged Al-Cu-Mg-Ag alloy

M.R. Gazizov [a,*], A.O. Boev [b], C.D. Marioara [c], R. Holmestad [d], M.Yu. Gazizova [a], R.
O. Kaibyshev [a]

[a] Belgorod State University, 308015 Belgorod, Russia
[b] Center for Energy Science and Technology, Skolkovo Institute of Science and Technology, 121205 Moscow, Russia
[c] Materials and Nanotechnology, SINTEF Industry, N-7465 Trondheim, Norway
[d] Department of Physics, Norwegian University of Science and Technology (NTNU), N-7491 Trondheim, Norway

ARTICLE INFO

ABSTRACT

The coherent edge interface structures of the relatively thin $\{111\}_{Al}$ Ω plates have been analyzed in a peak-aged Al-Cu-Mg-Ag alloy by atomic-resolution scanning transmission electron microscopy (STEM). Analysis of STEM images showed that these edge interfaces can deviate from their orthogonal orientations to the broad plate surfaces. The edge interface tilts correlate with orientations of the shear components appearing along the broad plate surfaces and changing with the plate thicknesses. Cu atoms tend to occupy specific atomic sites in the Al matrix region close to the edge interfaces.

1. Introduction

Al-Cu-Mg-Ag alloys exhibit high specific strength, good fracture toughness and fatigue fracture in addition to superior creep resistance at elevated temperatures. This is attributed to the uniformly dispersed Ω-phase formed during aging as well as its thermal resistance to coarsening [1–10].

Analysis of the precipitate microstructure in the peak- and over-aged alloys show that the Ω-phase has a plate-shaped morphology and lay on $\{111\}_{Al}$. The plates have a sandwich-like structure consisting of a core and broad interfaces [7,8,11–14]. Among a variety of structures proposed for the core, all of them are close to the equilibrium θ-phase (Al$_2$Cu, *I4/mcm*) [5,9,13–16]. Despite this fact, an orthorhombic structure has been the most widely accepted for the plates [7,8,13,14]. Orientation relationships for the orthorhombic Ω-phase were established to be $\{111\}_{Al}$ // $(001)_\theta$, $\langle110\rangle_{Al}//\langle010\rangle_\theta$ and $\langle211\rangle_{Al}//\langle100\rangle_\theta$ [8,9,14,17].

In Al-Cu-Mg-Ag alloys, the broad Al/Ω interfaces have a multilayered structure involving Ag and Mg atoms, segregations of which can be identified from the early aging stages [18]. Kang et al. suggested the energetically favorable Al/Ω interface configuration as seen from the Al matrix side to the precipitate interior is composed of Ag atoms in a hexagonal configuration (Ag atom arrangement similar to Al in the respectively substituted $\{111\}_{Al}$ layer), Mg atoms lying in the center of these hexagons yielding the stoichiometric composition of Ag$_2$Mg, and

then a Cu-enriched layer connected to the core orthorhombic θ lattice [7,12,19]. Yang et al. [20] showed by *ab initio* calculations that the Al can substitute Ag in the Ag$_2$Mg interface layers to form a slightly less energetically favorable precipitate structure compared to the latter. Thus, this fact can be directly linked to the presence of $\{111\}_{Al}$ Ω plates in Ag-free Al-Cu-Mg alloys [21,22]. It should be noted that the nature and/or evolution of the Ω phase is still not clearly explained in the literature. It is unclear whether the Ag and Mg atoms enveloping the broad surfaces of the Ω plates are a result of "segregation" (i.e., because of migration/diffusion of these atoms from the surrounding matrix to the interfaces of the Ω plates after its formation) or a result of rejection of these elemental atoms from within the clusters or precursors of Ω plates during their formation.

Despite considerable research interests to investigate the bulk Ω structure and the broad Ω/Al interfaces [7,8], its edge interfaces have rarely been analyzed. These edge interfaces were found to be predominantly free from Mg and Ag segregations compared to the broad plate interfaces. They are known to have coherent or semi-coherent (SC) structures depending on the plate thicknesses [3,8] and a smooth outward curvature at the relatively thick plates as observed in Fonda's work [3]. This curvature slightly varied among the various plate thicknesses. In Garg's [23], Fonda's [3] and Ringer's [9] work, three types of habit planes were classified for these edge interfaces as $\{110\}_{Al}$ // $\{010\}_\theta$ (type *A*), $\{110\}_{Al}$// $\{110\}_\theta$ (type *B*) and $\{211\}_{Al}$ // $\{100\}_\theta$ (type *C*) with their orthogonal orientation relative to the broad plate surfaces. Note

that type *C* can only be found on the rare octagonal-shaped Ω plates [23]. Moreover, the preferred plate lengthening direction was observed to be $[10-1]_{Al}$ // $[010]_\theta$ [9].

It is also interesting to note that Aaronson et al. [24] and Nie et al. [25] suggested that the formation of the plate-like precipitates such as Ω (Al_2Cu) in Al-Cu-Mg-Ag alloys and T1 (Al_2CuLi) in Al-Cu-Li alloys often is associated with a significant shear component at the broad interfaces. Strain accommodation mechanisms are known to play an important role to control both nucleation and growth of plate-like precipitates [2,8,26–30].

We confirmed in our recent work that there are structural and volumetric incompatibilities between the Al matrix and Ω plates [19,31]. Structural incompatibilities associated with the appearance of two shear components: $[-101]_{Al}$ // $[0-10]_\theta$ (τ_I) and $[1-21]_{Al}$ // $[100]_\theta$ (τ_{II}) can be along the broad interfaces of the plates with different thicknesses. The edge interface structures may indicate the presence of aforementioned shear components because the plates forming at the early aging stages tend to behave as elastically constrained thin films [8]. As the plate thickens during aging, the elastic properties of the plate would be expected to more closely approach those of the bulk [8] and elastic strain fields can be localized in the adjacent Al matrix. Analysis of the edge interfaces may shed light on strain field distributions around the $\{111\}_{Al}$ plates, knowing of which can help to understand mechanisms of $\{111\}_{Al}$ plate strengthening in aged aluminum alloys [10,32–34]; preferential Ω-phase orientations observed in the stress-aged Al-Cu-Mg-Ag alloys [27–30].

In the present work, we have studied the edge interface of the $\{111\}_{Al}$ Ω plates with thicknesses between 0 and 2 c_θ using atomic-resolution STEM. The relationships between orientations of the shear components appearing along the broad plate surfaces and the edge interface were found. There is a specific threshold thickness, when thin $\{111\}_{Al}$ plates tend to behave as elastically constrained thin films and elastic properties of thick ones approach more closely to the bulk Ω-phase.

2. Experimental procedure

An aluminum alloy with nominal chemical composition Al-4.5Cu-0.56 Mg-0.77Ag-0.42Mn- 0.12Ti-0.05 V-0.02Fe (in wt%) was prepared using a direct-chill, semi-continuous casting process. Initially, the alloy was homogenized at 500 °C for 24 h followed by cooling in a furnace. Further, the ingots were extruded at ~400 °C with a ratio of ~2.6 and hot-rolled to a reduction of ~60%. The samples were then solution heat treated at 510 °C for 1 h and quenched in water. Aging at 150 °C for 24 h and 190 °C for 1.5 h was carried out to provide peak-hardness state in the respective alloy [19,31].

TEM foils were prepared similarly as in [19,31] by electropolishing the ~150 μm thick samples using a solution of 2/3 methanol and 1/3 nitric acid at −30 °C. Foils were studied in two microscopes operated at 200 kV: a JEOL JEM-2100F and a double aberration corrected JEOL ARM-200F. The latter was equipped with a JEOL annular dark field (ADF) detector used in scanning mode [31]. A spot size of 0.08 nm, 27 mrad convergence semi-angle and collection semi-angles of 35–149 mrad were used as ADF-STEM presets. For some images, fast Fourier transform (FFT) filtering was applied to reduce noise with a periodicity shorter than ~0.05 nm.

The average plate diameters $\overline{D}_m$ and precipitate number density $\overline{N}_V$ as well as their standard deviations were estimated using TEM images in accordance with the methodology described in [19,32,35]. The foil thickness was measured by the convergent beam electron diffraction (CBED) method using Kossel-Möllenstedt fringes [36].

Crystal structures and elements occupying certain atomic columns were suggested from atomic-resolution ADF-STEM images containing atomic number (*Z*) contrast [37]. Therefore, ADF-STEM images taken in $\langle 211 \rangle_{Al}$ zone axes (ZAs) were acquired to analyze edge interfaces of

$\{111\}_{Al}$ Ω plates without overlapping with Al matrix along the respective viewing directions [3,9,23]. The VESTA software was used to analyze edge interface orientations [40].

Analysis of the atomic column arrangements performed in [19,31] showed that Ω plates are constructed from the broad interfaces and 'building blocks' based on an orthorhombic structure closely linked to the equilibrium θ-phase (Al_2Cu, *I4/mcm*) typical for the Ω phase [7,8,11–14]. Thus, the plate thicknesses (*t*) analyzed in the present work varied between 0 and 2 c_θ with the step of 0.5 c_θ in $[111]_{Al}$//$[001]_\theta$. Note that the thinnest Ω plates observed in the present work consist of interface layers of Ag_2Mg and Cu_i and a single Ω core layer Al_1 (or Al_2) parallel to the broad $\{111\}_{Al}$ plate surfaces, while a 0.5 c_θ cell should have the core layers arranged like …-Cu_m- Al_1(or Al_2)-Cu_m-… . For this reason the thinnest plates were hereinafter referred to 0 c_θ thick [31].

3. Results

3.1. Precipitate morphology

Careful analysis of the precipitate morphology was performed in the two samples peak-aged at 150 °C and 190 °C [19]. Examples of representative bright-field TEM images obtained with the electron beam parallel to $\langle 211 \rangle_{Al}$ zone axis (ZA), are shown in Fig. 1. In general, close examination reveals the presence of prevailing $\{111\}_{Al}$ Ω plates and
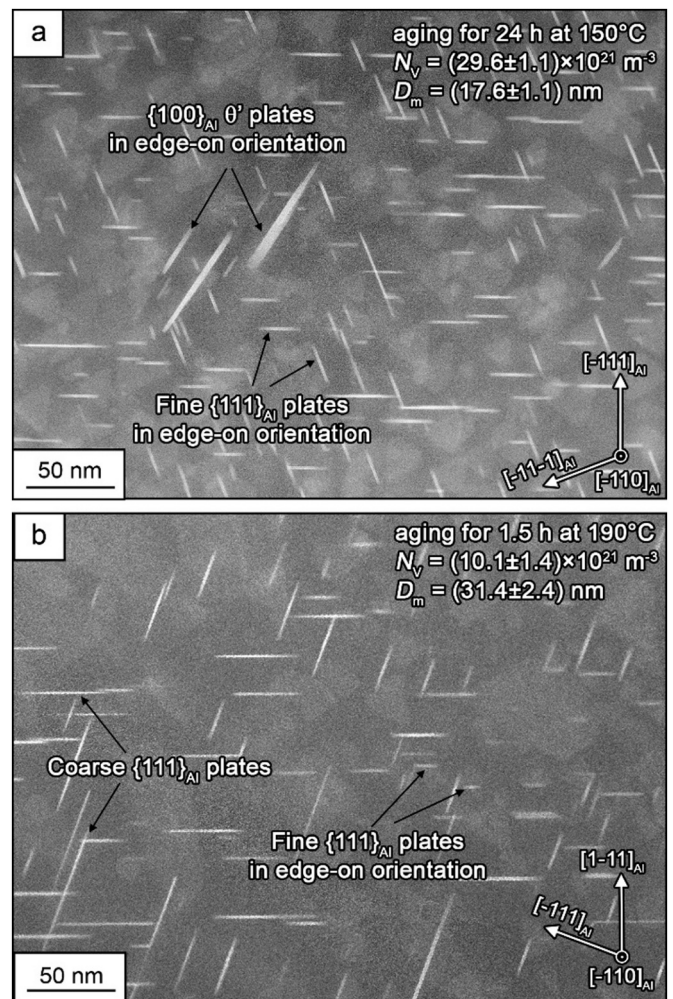

Fig. 1. ADF-STEM images taken along $\langle 110 \rangle_{Al}$ ZA representing typical grain interiors in the alloy peak-aged at 150 °C for 24 h (a) and 190 °C for 1.5 h (b). Average measured plate diameters $\overline{D}_m$ and precipitate number densities $\overline{N}_V$ are given for each condition.

minor fraction of $\{100\}_{Al}$ θ' plates in both peak-aging states. Statistical analysis showed that $\{111\}_{Al}$ Ω plates had twice as big average plate diameter and three times lower precipitate number density after peak-aging at 190 °C compared to aging at 150 °C [19,31]. The plate diameter distribution was found to be unimodal after aging at 150 °C in comparison with 190 °C, where the plate diameter distribution was bimodal [19,31]. The plate thickness distributions were quite narrow in both peak-aging stages with an average of 0.5 $c_θ$ [19,31].

3.2. High-resolution TEM analysis

The coherent edge interfaces of Ω plates are shown in Fig. 2. These ADF-STEM images represent the $\{111\}_{Al}$ plates in edge-on projections. Several structural features have been identified in these images. Firstly, the edge interface of the plates with thickness 0 $c_θ$ seems to be orthogonal to the broad plate surfaces (Fig. 2a). Fig. 2b and d show that the edge interfaces of non-hybrid Ω plates (involving only orthorhombic

θ-phase fragments [19,31]) with thicknesses in the range from 0.5 to 1 $c_θ$ are not orthogonal to the broad plate surfaces as described for the thick Ω plates in [3,9,23]. The edge interfaces are seen to be tilted by 60–65° from the broad interfaces in different viewing directions used to acquire the ADF-STEM images: $[-100]_θ$ and $[-110]_θ$. Considering ADF-STEM drift the edge interface of the hybrid Ω plates (involving orthorhombic θ- and hexagonal η-phase fragments [19]) with a thickness of about 0.5 $c_θ$ (Fig. 2c) and the non-hybrid precipitate with the thickness more than 1.5 $c_θ$ (Figs. 2e-g) were found to be perpendicular to the broad plate surfaces.

The relatively thick Ω plates analyzed in the present work have no misfit-compensating dislocation at the edge interfaces. Thus, their edge interfaces keep coherent structure with vacancy-type misfit strains normal to broad plate surfaces [3,8]. Note that a single misfit-compensating dislocation appears if the plate thickness increases to more than 3 $c_θ$ as shown in [3,8].
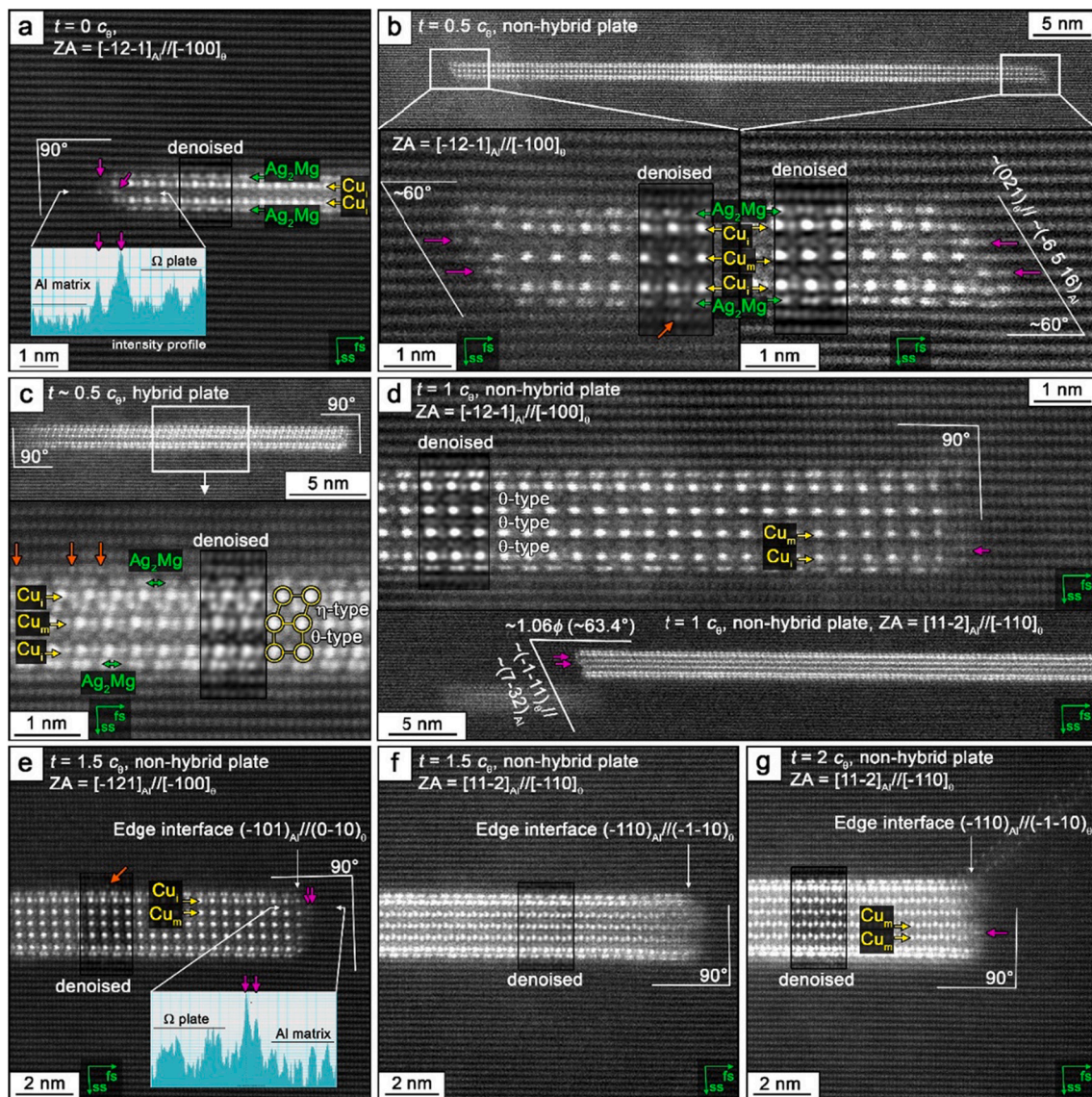
Fig. 2. The edge interfaces of the $\{111\}_{Al}$ Ω plates. The edge interfaces of 0.5 and 1 $c_θ$ thick plates are seen to deviate from the orthogonal orientation to the broad plate surfaces described for the thicker plates in [3,9,23]. The edge interface tilts seem to depend on the plate thickness, precipitate hybridization and viewing directions (projection planes) used to acquire ADF-STEM images. Note that the relatively thick Ω plates have the edge interfaces orthogonal to the broad plate surfaces. The brighter matrix atomic columns close to the edge and broad interfaces marked by the pink and red arrows, respectively, can be occupied with heavier elements like Cu ($Z = 29$) and Ag ($Z = 47$). The edge interfaces of the Ω-plates with the thickness up to 2 $c_θ$ are seen to be coherent with the Al matrix. FFT filtering (denoising) was applied in inserts. (For interpretation of the references to colour in this figure legend, the reader is referred to the web version of this article.)

4. Discussion

4.1. The coherent edge interface orientations

In Garg's [23], Fonda's [3] and Ringer's [9] work, the edge interfaces of the Ω plates in Al-Cu-Mg-Ag alloys aged at relatively high temperatures of 200–300 °C were observed to be generally orthogonal to the broad plate surfaces with curvatures varying slightly among various plate thicknesses. Our TEM observations (Fig. 2) support the fact that the coherent edge interfaces of the Ω plates forming in Al-Cu-Mg-Ag alloys under- and peak-aged at relatively low temperatures (150–190 °C) deviate from their orthogonal orientations observed in [3,9,23].

Crystallographic Ω/Al relationships and the hexagonal plate morphology are schematically represented in Fig. 3. It is seen that ADF-STEM images taken along <110>$_{Al}$ cannot provide a representative view of the hexagonal plate edge interface structures because they overlap with the Al matrix. Note that octagonal Ω plates were rarely found [3]. For this reason, we will hereinafter discuss the edge interface structures in terms of their common hexagonal morphology.

Relationships between the shear component orientations and the edge interface tilts will be considered with increasing plate thicknesses reflecting the precipitate evolution in the alloy during aging.

0 c_θ thick plates form at early aging stages and have shear component τ_{II} of 0.035 (Table 1) [31]. Despite this relatively large shear component τ_{II}, their edge interfaces seem to be orthogonal to the broad plate surfaces (Fig. 2a). We can suspect that these edge interfaces may be perpendicular to the broad plate surfaces because of unstable chemistry of the thin precipitates at early aging stages. Therefore, the bulk and interface structures of this thinnest Ω plates may be different from the orthorhombic θ lattice and Ag_2Mg/Cu_i interface layers given in literature [7,8,13,14]. Kang et al. [7] also suggested that certain atomic columns in the Ag_2Mg layers can be enriched by other elements like Al or Cu, due to strain accommodation and interface energy minimization mechanisms activated by an incompatibility between precipitate and

Table 1
Relationships between the plate thicknesses (*t*), shear components (τ_I [−101]$_{Al}$ //[0–10]$_\theta$ or τ_{II} [1–21]$_{Al}$ //[100]$_\theta$) and edge interface orientations. Shear components and misfit strains were parametrized for the plates with different thicknesses in [31]. Note that examples of the edge interface orientations are shown in cross-sections *A-A*, …, *D*-D** in Fig. 3.

t, c_θ	Shear components	Misfit strain in [111]$_{Al}$	Edge interfaces in hexagonal Ω plates	
			Type A	Type B
0	$\tau_{II} = 0.035$	−0.019	(10–1)$_{Al}$// (010)$_\theta$[b]	(1–10)$_{Al}$//(−110)$_\theta$; (01–1)$_{Al}$//(110)$_\theta$[b]
0.5	$\tau_I = 0.024$	−0.026	~(−6 5 16)$_{Al}$/(021)$_\theta$ (*A-A*)	~(15–3)$_{Al}$// ~(−2−21)$_\theta$ (*B—B*); ~(5–31)$_{Al}$//~ (2–21)$_\theta$ (*B*-B**)
	$\tau \sim 0$ for hybrid plates	n.a.	(10–1)$_{Al}$// (010)$_\theta$[b]	(1–10)$_{Al}$//(−110)$_\theta$; (01–1)$_{Al}$//(110)$_\theta$[b]
1	τ_I[a]	_[a]	_[a]	_[a]
	$\tau_{II} = 0.028$	−0.024	(10–1)$_{Al}$// (010)$_\theta$[b] (*C—C*)	~(7–3 2)$_{Al}$//~(−1–11)$_\theta$ (*D—D*); ~(2–3 7)$_{Al}$//~ (1–11)$_\theta$ (*D*-D**)
1.5	$\tau_{II} = 0.010$	−0.032	(10–1)$_{Al}$// (010)$_\theta$[b]	(1–10)$_{Al}$//(−110)$_\theta$; (01–1)$_{Al}$//(110)$_\theta$[b]
2	$\tau_{II} \sim 0.002$	−0.034	(10–1)$_{Al}$// (010)$_\theta$[b]	(1–10)$_{Al}$//(−110)$_\theta$; (01–1)$_{Al}$//(110)$_\theta$[b]

[a] 1 c_θ thick plates with shear component τ_I were not observed in TEM despite their structures were found to have the same formation enthalpy as 1 c_θ thick plates with τ_{II} [31].

[b] The edge interface orientations are initially given in [23]

matrix lattices. For instance, atomic segregations in Al matrix regions adjacent to the broad plate surfaces are marked by red arrows in Fig. 2c.

Among 0.5 c_θ thick plates prevailing in the alloys peak-aged at 150 °C and 190 °C [19,31], there are several precipitate configurations: non-hybrid (involving only orthorhombic θ-phase fragments) and hybrid structures (involving θ- and hexagonal η-phase fragments) with number fractions of ~0.94 and 0.88 after peak-aging at 150 °C and 190 °C,
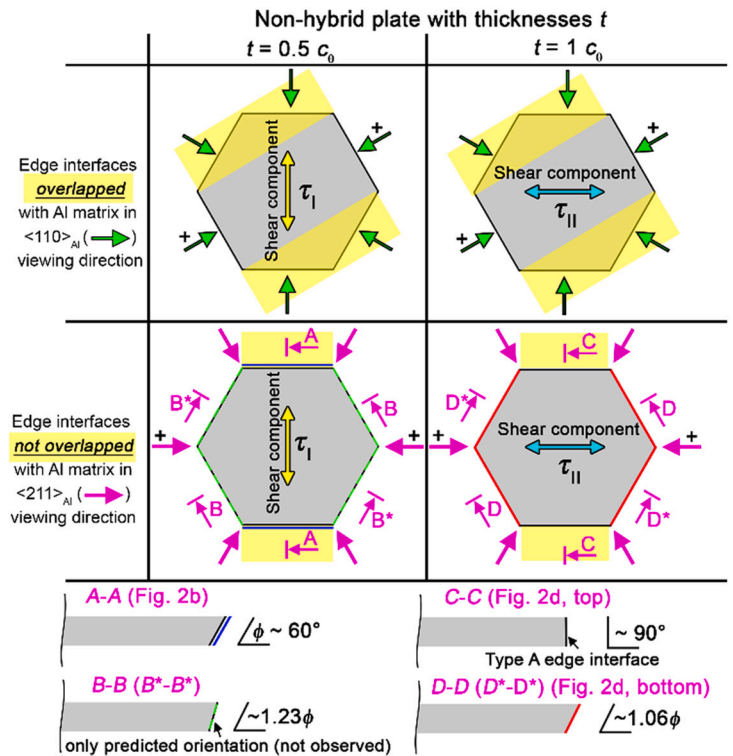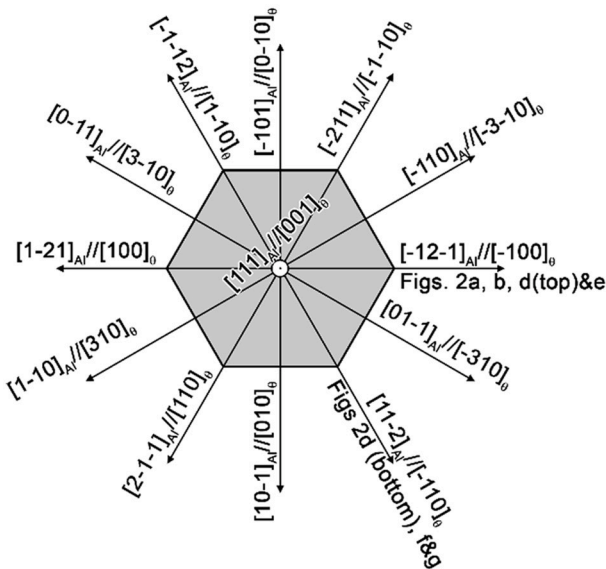
Fig. 3. Schematic representation of the precipitate geometry, the edge interface and shear component orientations in different crystallographic projections. [−101]$_{Al}$ // [0–10]$_\theta$ and [1–21]$_{Al}$ // [100]$_\theta$ shear components were designated as τ_I and τ_{II}, respectively. Examples of the regions with and without the edge interface overlapping with the adjacent Al matrix along some viewing directions marked by '+' are shown.

respectively [19,31]. Note that the hybrid plates have a shear component close to zero caused by hybridization providing high precipitate/matrix structural compatibility [19]. As a result, a good structural compatibility led to an orthogonal orientation of their edge interfaces relative to the broad plate surfaces (Fig. 2c).

Rarely observed non-hybrid 0.5 c_θ thick plates are known to be energetically favorable, with $[1–21]_{Al}$ // $[100]_\theta$ shear component (τ_I) of 0.024 (Table 1) [31]. These plates are seen in Fig. 2b to have the edge interfaces deviated from the orthogonal $(010)_\theta$ //$(10–1)_{Al}$ habit plane (type *A*) found in the thicker Ω plates in the present work (Fig. 2e-g) and literature [3,23]. A rough estimation of these edge interface orientations yields the tilting angle (φ) of ~60° and the habit plane ~$(021)_\theta$ // ~$(–6\ 5\ 16)_{Al}$ in $[−12−1]_{Al}$ // $[−100]_\theta$ viewing direction or cross-sections *A-A* as shown in Fig. 3.

Type *B* edge interfaces with $\{110\}_{Al}$// $\{110\}_\theta$ habit planes [3,23] should also deviate from their orthogonal orientation to the broad plate surfaces in *B—B* and *B*-B** cross-sections (Fig. 3). Note that these interfaces have not been observed. They should be tilted by ~73.8° to the broad plate surfaces and have habit planes ~$(1\ 5–3)_{Al}$//~$(−2−21)_\theta$ and ~ $(5–3\ 1)_{Al}$//~$(2–21)_\theta$ in cross-sections *B—B* and *B*-B**, respectively (Table 1). These edge interface deviations can be related to the τ_I shear component, directions of which do not lie in $[2−1−1]_{Al}$ and $[11−2]_{Al}$ projection planes (Fig. 3).

1 c_θ thick plates can have energetically favorable shear components τ_I and τ_{II} [31]. The main difference between 1 c_θ thick plates with τ_I and τ_{II} was that in the former case the supercell modelled and calculated by density functional theory (DFT) had larger τ_I and smaller misfit strain in $[111]_{Al}$ in comparison with the latter one. Low energy states in both supercells were provided by balances between shear and misfit strains because increase in the interplane spacing ($d_{[111Al]}$) promoted reducing shear strain field energy (E_S) being inversely proportional to $d_{[111Al]}$ (E_S ~ $1 / d_{[111Al]}$) [19,31,38]. Note that the periodic boundary conditions were used in [31]. As a result, DFT supercells included infinite $\{111\}_{Al}$ Ω plates [31]. It seems that the finite plates embedded to the Al matrix in practice tend to reduce the shear strain more than misfits in $[111]_{Al}$. We did not observe 1 c_θ thick plates with τ_I in our TEM samples perhaps because of this plate/shear component configuration can be quite rare.

For 1 c_θ thick plates with τ_{II}, there are two possible viewing directions the edge interfaces without overlapping with the Al matrix. At first, the shear component τ_{II} cannot be clearly projected in the *C—C* cross-section as seen in viewing direction $[1−21]_{Al}$ // $[100]_\theta$ in Fig. 2d (top). This occurs because the direction of the shear component τ_{II} is perpendicular to the projection plane. Secondly, the tilted edge interface can be seen in directions $[11−2]_{Al}$ // $[−110]_\theta$ (cross-section *D-D*) and $[2−1-1]_{Al}$ // $[110]_\theta$ (*D*-D**). The edge interface tilts are estimated to be ~63.4° (or ~ 1.06φ) relative to the broad plate surfaces in both cross-sections. A rough estimation yields the habit planes to be ~$(7–32)_{Al}$//~$(−1−11)_\theta$ and ~ $(2–37)_{Al}$//~$(1–11)_\theta$ seen in *D—D* and *D*-D** cross-sections, respectively (Fig. 3, Table 1). Thus, type B edge interfaces also deviate from orthogonal orientations observed in [3,23].

1.5 and 2 c_θ thick plates with shear components τ_{II} of 0.010 and 0.002, respectively [31], have the coherent edge interfaces with habit planes consistent with type *A* and *B* edge interface orientations [3,23]. It should be noted that their curvatures are close to zero (Figs. 2e-g) in comparison with the thick plates shown in [3,23].

Thus, we can conclude that the edge interface tilts of the relatively thin plates forming at early aging stages correlate with the shear component directions depending on the plate thickness in the range from 0.5 to 1 c_θ. Taking into account that interface orientations and forces acting on the precipitate surfaces as well as in its bulk are interdependent [26] we can conclude that very small plates tend to behave like elastically constrained thin films. This phenomenon was predicted for the Ω plates in [8]. The habit planes of coherent edge interfaces for the plates with thicknesses from 0 to 1 c_θ are different from those for the thicker plates analyzed in the present work and initially described in [3,9,23].

It should be noted that our TEM observations did not support the fact that the edge interface orientations can be directly linked to peculiarities in the plate diameter distributions found in the experimental alloy peak-aged at 150 °C and 190 °C [19,31].

4.2. Cu atom occupations in the Al matrix regions close to the plate tips

Analysis of the ADF-STEM image intensity distributions for atomic columns at the Ω plate tips showed that heavier elements (because of brighter atomic columns compared to the surrounding Al matrix) tend to occupy sites in the Al matrix close to the coherent edge interfaces. This occurs out of the plate in Al_1 or Al_2 planes as marked by the yellow arrows in Figs. 2a, b, e and g). This phenomenon seems not to depend on the plate thicknesses or shear component directions.

Because of volumetric precipitate/matrix incompatibilities as well as absence of misfit-compensating dislocations at the edge interfaces, vacancy-type uncompensated misfits are present in $[111]_{Al}$//$[001]_\theta$ normal to the broad plate surfaces [8,13,22,23]. The compression strain field appears in the adjacent Al matrix regions close to the coherent edge interface. These uncompensated misfit strains gradually increase with the plate thickness until misfit-compensating dislocations appear. For this reason, we can conclude that smaller Cu atoms (r_{Cu} = 0.128 nm [39]) tend to segregate in the respective Al matrix columns (r_{Al} = 0.143 nm [39]) in comparison with other alloying elements such as Ag (r_{Ag} = 0.145 nm [39]) and Mg (r_{Mg} = 0.160 nm [39]).

Cu presence near the edge interfaces can be linked to a necessary mass transfer phenomenon, or to its local equilibrium concentration. Since the experiment are done in the peak-aged state of the alloy, the Ω precipitates are in the growth stage. It requires Cu incorporation into internal θ structure of the Ω plates to support their lengthening process. Note that Cu tends to occupy specific sites in the Al matrix, which are located as continuations of the precipitate Cu-free Al_1 and Al_2 planes (Fig. 2a, b, d, e and g). If this is a mass transfer process for Cu, a splitting of its diffusional pathway to neighbor Cu_m (or/and Cu_i) layers is required to incorporate this element into the bulk θ structure.

5. Conclusion

The edge interfaces of the $\{111\}_{Al}$ Ω plates with thicknesses up to 2 c_θ have been analyzed in an Al-Cu-Mg-Ag alloy peak-aged at 150 °C for 24 h and 190 °C for 1.5 h by aberration-corrected STEM. The edge interfaces of 0 c_θ thick plates formed at early aging stages and probably having the largest shear component (0.035) have been found to be orthogonal to the broad plate surfaces because of their unstable chemistry at early aging stages. The edge interfaces of non-hybrid 0.5 and 1 c_θ thick plates with shear components of 0.024 and 0.028, respectively, are tilted by 60–65° to the broad plate surfaces. The plates thicker than 1.5 c_θ with shear components less than 0.010 as well as hybrid 0.5 c_θ thick Ω plates involving orthorhombic θ- and hexagonal η-phase fragments with the shear component close to zero, have the edge interfaces orthogonal to the broad plate surfaces.

Cu atoms occupy specific sites located in the Al matrix near the edge Ω/Al interfaces and on continuations of the precipitate Cu-free Al_1 and Al_2 planes. This feature can be linked to a necessary mass transfer phenomenon related to precipitate growth, or to its local equilibrium concentration.

Declaration of Competing Interest

The authors declare that they have no known competing financial interests or personal relationships that could have appeared to influence the work reported in this paper.

Data availability

The raw/processed data required to reproduce these findings cannot be shared at this time as the data also forms part of an ongoing study.

References

[1] I.J. Polmear, Light Alloys: From Traditional Alloys to Nanocrystals, third ed., Butterworth-Heinemann/Elsevier, Oxford (UK), 2006.

[2] J.F. Nie, Physical metallurgy of light alloys, in: Phys. Metall, Fifth Ed, Elsevier, 2014, pp. 2009–2156, https://doi.org/10.1016/B978-0-444-53770-6.00020-4.

[3] R.W. Fonda, W.A. Cassada, G.J.J. Shiflet, Accommodation of the misfit strain surrounding {III} precipitates (Ω) in Al-Cu-Mg-(Ag), Acta Metall. Mater. 40 (1992) 2539–2546.

[4] K.M. Knowles, W.M. Stobbs, The structure of {111} age-hardening precipitates in Al–Cu–Mg–Ag alloys, Acta Crystallogr. Sect. B Struct. Sci. 44 (1988) 207–227, https://doi.org/10.1107/S0108768187012308.

[5] J.H. Auld, Structure of metastable precipitate in some Al–Cu–Mg–Ag alloys, Mater. Sci. Technol. 2 (1986) 784–787, https://doi.org/10.1179/mst.1986.2.8.784.

[6] S. Kerry, V.D. Scott, Structure and orientation relationship of precipitates formed in Al-Cu-Mg-Ag alloys, Met. Sci. 18 (1984) 289–294, https://doi.org/10.1179/030634584790420069.

[7] S.J. Kang, Y.W. Kim, M. Kim, J.M. Zuo, Determination of interfacial atomic structure, misfits and energetics of Ω phase in Al-Cu-Mg-Ag alloy, Acta Mater. 81 (2014) 501–511, https://doi.org/10.1016/j.actamat.2014.07.074.

[8] C.R. Hutchinson, X. Fan, S.J. Pennycook, G.J. Shiflet, On the origin of the high coarsening resistance of Ω plates in Al–Cu–Mg–Ag Alloys, Acta Mater. 49 (2001) 2827–2841, https://doi.org/10.1016/S1359-6454(01)00155-0.

[9] S.P. Ringer, W. Yeung, B.C. Muddle, I.J. Polmear, Precipitate stability in AlCuMgAg alloys aged at high temperatures, Acta Metall. Mater. 42 (1994) 1715–1725, https://doi.org/10.1016/0956-7151(94)90381-6.

[10] M. Gazizov, R. Kaibyshev, Low-cyclic fatigue behaviour of an Al-Cu-Mg-Ag alloy under T6 and T840 conditions, Mater. Sci. Technol. (United Kingdom). 33 (2017), https://doi.org/10.1080/02670836.2016.1163876.

[11] L. Sun, D.L. Irving, M.A. Zikry, D.W. Brenner, First-principles investigation of the structure and synergistic chemical bonding of Ag and Mg at the Al|Ω interface in a Al-Cu-Mg-Ag alloy, Acta Mater. 57 (2009) 3522–3528, https://doi.org/10.1016/j.actamat.2009.04.006.

[12] S.J. Kang, J.-M. Zuo, H.N. Han, M. Kim, Ab initio study of growth mechanism of omega precipitates in Al-Cu-Mg-Ag alloy and similar systems, J. Alloys Compd. 737 (2018) 207–212, https://doi.org/10.1016/J.JALLCOM.2017.12.010.

[13] B.C. Muddle, I.J. Polmear, The precipitation Ω phase in Al-Cu-Mg-Ag alloys, Acta Metall. 37 (1989) 777–789, https://doi.org/10.1016/0001-6160(89)90005-9.

[14] S.C. Wang, M.J. Starink, Precipitates and intermetallic phases in precipitation hardening Al–Cu–Mg–(Li) based alloys, Int. Mater. Rev. 50 (2005) 193–215, https://doi.org/10.1179/174328005X14357.

[15] S. Kerry, V.D. Scott, Structure and orientation relationship of precipitates formed in Al-Cu-Mg-Ag alloys, Met. Sci. 18 (1984) 289–294, https://doi.org/10.1179/030634584790420069.

[16] S. Abis, P. Mengucci, G. Riontino, A study of the high-temperature ageing of Al-Cu-Mg-Ag alloy 201, Philos. Mag. B Phys. Condens. Matter; Stat. Mech. Electron. Opt. Magn. Prop. 67 (1993) 465–484, https://doi.org/10.1080/13642819308207686.

[17] D. Vaughan, J.M. Silcock, The orientation and shape of θ precipitates formed in an Al-Cu alloy, Phys. Status Solidi 20 (1967) 725–736, https://doi.org/10.1002/pssb.19670200235.

[18] L. Reich, M. Murayama, K. Hono, Evoultion of Ω phase in an Al-Cu-Mg-Ag alloy - a three dimensional atom probe study, Acta Mater. 46 (1998) 6053–6062.

[19] M.R. Gazizov, A.O. Boev, C.D. Marioara, S.J. Andersen, R. Holmestad, R.O. Kaibyshev, D.A. Aksyonov, V.S. Krasnikov, The unique hybrid precipitate in a peak-aged Al-Cu-Mg-Ag alloy, Scr. Mater. 194 (2021), 113669, https://doi.org/10.1016/j.scriptamat.2020.113669.

[20] S.L. Yang, N. Wilson, J.F. Nie, Revisit of the structure of Ω precipitate in Al-Cu-Mg-Ag alloys, Scr. Mater. 205 (2021), 114204, https://doi.org/10.1016/j.scriptamat.2021.114204.

[21] A. Garg, Y.C. Chang, J.M. Howe, Precipitation of the Ω phase in an Al-4.0Cu-0.5Mg alloy, Scr. Metall. Mater. 24 (1990) 677–680, https://doi.org/10.1016/0956-716X(90)90222-3.

[22] S.P. Ringer, K. Hono, I.J. Polmear, T. Sakurai, Nucleations of precipitates in aged Al-Cu-Mg-(Ag) alloys with high Cu:Mg ratios, Acta Mater. 44 (1996) 1883–1898.

[23] A. Garg, J.M. Howe, Convergent-beam electron diffraction analysis of the Ω phase in an Al-4.0Cu-0.5Mg-0.5Ag alloy, Acta Metall. Mater. 39 (1991) 1939–1946.

[24] H.I. Aaronson, B.C. Muddle, J.F. Nie, On recent developments in the debate about the formation mechanism of precipitate plates, Scr. Mater. 41 (1999) 203–208, https://doi.org/10.1016/S1359-6462(99)00144-X.

[25] J.F. Nie, H. Aaronson, B.C. Muddle, The formation of precipitate plates and their role in the strengthening of aluminium alloys, in: M. Tiyakioglu, M. Tiyakioglu (Eds.), Adv. Metall. Alum. Alloy., Indianapolis, 2001, pp. 229–238.

[26] D.A. Porter, K.E. Easterling, M.Y. Sherif, Phase Transformations in Metals and Alloys, third ed., CRC Press, New York, 2014.

[27] J. Chen, C. Liu, Q. Li, H. Zhao, A three-dimensional characterization method for the preferentially oriented precipitation of Ω-phase in stress-aged Al-Cu-Mg-Ag single crystal, Mater. Charact. 153 (2019) 184–189, https://doi.org/10.1016/j.matchar.2019.04.035.

[28] B. Skrotzki, G.J. Shiflet, E.A. Starke, On the Effect of Stress on Nucleation and Growth of Precipitates in an Al-Cu-Mg-Ag Alloy 27 (1996).

[29] S. Muraishi, S. Kumai, A. Satoy, Stress-oriented nucleation of Ω-phase plates in an Al - Cu - Mg - Ag alloy, Philos. Mag. A. 82 (2002) 415–429.

[30] S. Bai, Z. Liu, X. Zhou, P. Xia, M. Liu, Stress-induced thickening of Ω phase in Al–Cu–Mg alloys containing various Ag additions, Mater. Sci. Eng. A 589 (2014) 89–96, https://doi.org/10.1016/j.msea.2013.09.065.

[31] M.R. Gazizov, A.O. Boev, C.D. Marioara, R. Holmestad, D.A. Aksyonov, M.Yu. Gazizova, R.O. Kaibyshev, Precipitate/matrix incompatibilities related to the {111}Al Ω plates in an Al-Cu-Mg-Ag alloy, Mater. Charact. 182 (2021), 111586, https://doi.org/10.1016/j.matchar.2021.111586.

[32] M. Gazizov, R. Kaibyshev, Precipitation structure and strengthening mechanisms in an Al-Cu-Mg-Ag alloy, Mater. Sci. Eng. A 702 (2017) 29–40, https://doi.org/10.1016/j.msea.2017.06.110.

[33] J. da Costa Teixeira, D.G. Cram, L. Bourgeois, T.J. Bastow, A.J. Hill, C.R. Hutchinson, On the strengthening response of aluminum alloys containing shear-resistant plate-shaped precipitates, Acta Mater. 56 (2008) 6109–6122, https://doi.org/10.1016/j.actamat.2008.08.023.

[34] J.F. Nie, B.C. Muddle, Microstructural design of high-strength aluminum alloys, J. Phase Equilib. 19 (1998) 543–551, https://doi.org/10.1361/105497198770341734.

[35] J.F. Nie, B.C. Muddle, Strengthening of an Al–Cu–Sn alloy by deformation-resistant precipitate plates, Acta Mater. 56 (2008) 3490–3501, https://doi.org/10.1016/j.actamat.2008.03.028.

[36] D.B. Williams, B.C. Carter, Transmission Electron Microscopy: A Textbook for Materials Science, 2nd ed., Springer, New York, 2009.

[37] P.D. Nellist, S.J. Pennycook, in: P.W. Hawkes (Ed.), The principles and interpretation of annular dark-field Z-contrast imaging, Elsevier, 2000, pp. 147–203, https://doi.org/10.1016/S1076-5670(00)80013-0.

[38] R.W.K. Honeycombe, The Plastic Deformation of Metals, 2nd ed., Hodder Arnold, New York, 1984.

[39] R.E. Smallman, A.H.W. Ngan, Atoms and atomic arrangements, in: Mod. Phys. Metall, Elsevier, 2014, pp. 1–41, https://doi.org/10.1016/b978-0-08-098204-5.00001-8.

[40] K. Momma, F. Izumi, *VESTA3* for three-dimensional visualization of crystal, volumetric and morphology data, J. Appl. Cryst. 44 (2011) 1272–1276, https://doi.org/10.1107/S0021889811038970.